In: Proceedings of the 17th European Biomass Conference & Exhibition,
June/July 2009, Hamburg, ETA-Renewable Energies (Ed.), Italy

UPDRAFT FIXED-BED GASIFICATION OF SOFTWOOD PELLETS: MATHEMATICAL MODELLING AND COMPARISON WITH EXPERIMENTAL DATA

C. Mandl[1] I. Obernberger[1,2], F. Biedermann[2]
[1]Graz University of Technology, Institute for Process and Particle Engineering,
Inffeldgasse 21b, A-8010 Graz, Austria
Tel.: +43 (0)316 873 4894, Fax: +43 (0)316 873 104894; E-mail: christoph.mandl@tugraz.at
[2]BIOS BIOENERGIESYSTEME GmbH, Inffeldgasse 21b, A-8010 Graz, Austria

ABSTRACT: This paper presents a one dimensional steady state mathematical model for the simulation of a small scale fixed-bed gasifier. The model is based on a set of differential equations describing the entire gasification process of softwood pellets and is solved by a two step iterative method. The main features of the model are: homogeneous and heterogeneous combustion and gasification reactions, one step global pyrolysis kinetics and drying, heat and mass transfer in the solid and gas phases as well as between phases, heat loss, particle movement and shrinkage within the bed. The model is used to simulate a laboratory scale fixed-bed updraft gasifier. Good agreement is achieved between prediction and measurements for the axial temperature profiles. The prediction of the composition and particularly of the tar content of the producer gas is imprecise due to insufficient data regarding the product composition of primary pyrolysis of softwood pellets. Therefore, the tar ratio of the primary pyrolysis reaction has been reduced and the remaining reported tar ratio undergoes a secondary reaction forming lighter gases and finally the model is in good agreement with experimental data.
Keywords: modelling, gasification, fixed bed, wood pellet

1 INTRODUCTION

The gasification of renewable solid biomass to produce CO_2-neutral fuels for heat and electricity production is still in the development stage. Softwood pellets are presently used in small-scale residential combustion units and the market will further increase within the next years, pellets may also be used in small-scale fixed-bed gasifiers for heating purposes as well as regarding micro-CHP applications (e.g. Stirling engine or micro-turbine). Due to the high tar content of the producer gas (up to 150 g/m³), updraft gasifiers are not suitable for engines and gas turbines without comprehensive gas cleaning. Since appropriate models for the proper design of such gasifiers and for a better understanding of the gasification process are needed, this paper presents a one-dimensional mathematical model.

Various models [1-7] dealing with the simulation of updraft fixed-bed gasifiers can be found in literature, but some of them are quite old or contain simplifying assumptions regarding physical properties and kinetics. Furthermore, the majority of the models have been applied to the gasification of coal. Focusing on the gasification of softwood pellets, only one model has been proposed so far [3]. An important fact is that mathematical models often contain complex differential equations resulting in extensive numerical solutions. One possibility to reduce the complexity of the numerical solution is to use time-independent mathematical models, which is acceptable when focusing on steady state operation. However, a description of the dynamic behaviour of the gasifier, which is primarily relevant for control purposes, is not possible. The scope of this work is the modelling of the steady state operation of a fixed-bed gasifier operated with softwood pellets with respect to proper reactor design and influence of changed operating conditions on the gasification process. Also, experiments have been carried out with a lab-scale gasifier and a comparison between model predictions and measurements is provided.

2 MATHEMATICAL MODEL

Figure 1 shows the basic geometry of the updraft gasifier presented in this paper.

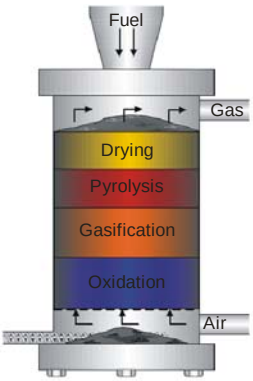

Figure 1: Fixed-bed updraft gasifier

The fuel (pellets) is fed continuously from the top of the gasifier, which can be considered as a simple cylindrical shaft, and forms a packed bed on the grate. The gasification air is injected from the bottom below the grate and passes through the fuel bed. Hot product gases exit the gasifier from the top, while the pellets descent toward the grate and are heated up successively by the gases. The fuel ash falls through the grate. The overall gasification process can be separated into four different reaction zones stratified along the reactor height – drying, pyrolysis, gasification and combustion. On the gasifier top the fuel is heated up by the hot gases and evaporation of fuel moisture usually starts immediately. Above temperatures of around 425K pyrolysis of the fuel takes place and char particles and volatiles are formed. The char particles move downwards, heat up and get reduced by hot gases as gasification processes start above approximately 1000K. Finally the char is oxidised by the supplied air at the bottom of the gasifier, supplying heat necessary for the overlying processes.

2.2 Governing equations

The gasification process is modelled by means of governing equations of the solid and gas phase. The equations are one-dimensional differential mass and energy balances on the solid and the gas phase. However, radial gradients exist. But, due to the fact that the residence time of the solids in the bed is long, radial gradients can be neglected. The general form (Eq. 1) of the energy equation is

$$\frac{\partial u}{\partial t}+\frac{\partial s_h}{\partial x}+s_q=\frac{\partial}{\partial x}(\lambda*\frac{\partial T}{\partial x}) \quad (1)$$

On the left side of Eq.1 the first term is the storage term, the second is the transport term and the third term is the transfer term [8]. The term on the right-hand side of the equation is the diffusion term. As mentioned before this paper focuses on steady-state operation, consequently the storage term is not considered. The transfer term contains the heat loss through the reactor walls, the solid to gas heat transfer and the heat flux due to chemical reaction and for the solid phase the evaporation enthalpy. Some previous models assume that the gas and solid temperature in a packed bed are equal, which is incorrect as shown by other authors [1, 11, 12]. Therefore, separate equations for the solid and the gas phase are required.
The energy equation for the solid phase is

$$-\frac{\partial}{\partial z}(\rho_{solid}*cp_{solid}*T_{solid}*v_{solid})=\frac{\partial}{\partial z}\left(\lambda_{solid}\frac{\partial T_{solid}}{\partial z}\right)- \quad (2)$$

$$\sum r_{i,solid}*\Delta H_{r,solid}-W_{sg}+W_{ws}$$

and the energy equation for the gas phase is

$$\frac{\partial}{\partial z}(\rho_{gas}*cp_{gas}*T_{gas}*v_{gas})=\frac{\partial}{\partial z}\left(\lambda_{gas}\frac{\partial T_{gas}}{\partial z}\right)- \quad (3)$$

$$\sum r_{i,gas}*\Delta H_{r,gas}+W_{sg}+W_{wg}$$

The heat loss through the reactor walls is not negligible and is considered according to [4]

$$W_{w,i}=\frac{4*\alpha_w}{D_V}*(T_w-T_i) \quad (4)$$

The heat transfer [21] between the solid and the gas phase is evaluated according to equation 5.

$$W_{sg}=\zeta*\frac{2.06*cp_{gas}*\rho_{gas}*v_{gas}}{\varepsilon}*\mathrm{Re}^{-0.575}*\mathrm{Pr}^{-\frac{2}{3}}*A_P*(T_S-T_g) \quad (5)$$

A dimensionless correction factor ζ has been introduced before [1, 6] to account for uncertainties regarding physical characteristics of the biomass and heat transfer effects in reacting systems. The packed bed at any point is described by the specific surface area (A_P) and the void fraction ε. Assuming that no fragmentation and agglomeration of particles take place in the reactor, the void fraction is supposed to be constant. The specific surface area (A_P) depends on the actual equivalent diameter of the biomass particles and the void fraction of the bed and can be evaluated from equation 6 [11].

$$A_P=\frac{6*(1-\varepsilon)}{d_p} \quad (6)$$

The equivalent diameter of the biomass particles and consequently the speed of the biomass are assumed to remain constant along the drying and pyrolysis zones, while the density of the biomass decreases. On the contrary, due to the heterogeneous reactions in the gasification and oxidation zone, the diameter of the biomass particles and the speed of the biomass decrease accordingly to the unreacted-core model with shrinking particle size [11], while the density of the biomass char remains constant.

The conservation equations are considered for the solid and the gas phase species. For the solid phase the species biomass (wood pellets) and char are derived, the gas phase species are H_2O, CO, CO_2, H_2, CH_4, tar, O_2 and N_2. Furthermore, the fuel moisture is considered to be a part of the solid phase.

$$\frac{\partial}{\partial z}(v_{solid}*\rho_{wood})=-r_{wood} \quad (7)$$

$$\frac{\partial}{\partial z}(v_{solid}*\rho_{char})=-\sum r_{i,char} \quad (8)$$

$$\frac{\partial}{\partial z}(v_{solid}*\rho_{moisture})=-m_{water} \quad (9)$$

The superficial velocity of the char in bulk can be evaluated from Eq. 10.

$$\frac{\partial v_{solid}}{\partial z}=-\frac{1}{\rho_{char,0}}*\sum r_{i,char} \quad (10)$$

In the formulation of the conservation equation of the gas phase species turbulence and diffusion are not considered, thus the general form of the conservation equation of the gas phase species is

$$\frac{\partial \rho_{i,gas}}{\partial z}=\frac{1}{v_{gas}}*\left(r_{i,gas}-\rho_{i,gas}*\frac{\partial v_{gas}}{\partial z}\right) \quad (11)$$

In the model approach the gasifier is assumed to be isobaric. However, the pressure drop is expected not to be negligible, primarily when a thick layer of ash is built up on the grate as it could be observed during experiments. On the other hand, the pressure drop of a packed bed of softwood pellets is supposed to be relatively small compared to the pressure drop caused by the ash layer. Furthermore, a thick ash layer may have a significant influence on the gasification process as shown in [11].Thus, for all simulations carried out the ash layer is supposed to be small as the ash is periodically removed from the grate.
The speed of the gas phase can be evaluated from the continuity equation (Eq. 12) of the gas phase.

$$\frac{\partial}{\partial z}(\rho_{i,gas}*v_{gas})=\sum r_{i,gas}+m_{water} \quad (12)$$

2.3 Kinetics

The overall gasification process can be separated into four different reaction zones stratified along the reactor height. For each zone the main physical properties and chemical reactions are considered by the model.

2.3.1 Drying

The drying process of the biomass is described by a 1st order kinetic equation depending on the temperature of the solid by means of an Arrhenius kind expression (Eq. 13) [10]. Kinetic constants are derived from [10] and are listed in Table II.

$$m_{water}=(1-\varepsilon)*(\rho_{solid}-\rho_{solid,dry})*A_{H_2O}*\exp\left(-\frac{E_{H_2O}}{R*T_{solid}}\right) \quad (13)$$

2.3.2 Pyrolysis

The devolatilization of biomass is a complex phenomenon, which involves a large number of chemical reactions. As usually done in mathematical modelling of fixed-bed reactors, pyrolysis is described by an one-step global reaction (Eq.14).

$$r_{p1} = \rho_{wood,dry} * A_{p1} * \exp\left(\frac{E_{p1}}{R * T_{solid}}\right) \quad (14)$$

The considered products of the global reaction are as following (Eq. 15).

$$biomass \rightarrow CO + CO_2 + H_2O + CH_4 + H_2 + tar + char \quad (15)$$

Tars often undergo secondary cracking reactions (r_{p2}) to form combustible gases (CO, CH_4), CO_2 and water vapour [15].

$$r_{p2} = W_{tar} * A_{p2} * \exp\left(-\frac{E_{p2}}{R * T_{gas}}\right) \quad (16)$$

Condensation of tars is not considered, since the chemical composition and therefore the dew point of the tars are unknown. Furthermore, the temperatures in the upper fuel bed are expected to be relatively high due to the low moisture content of softwood pellets, so that most of the tars exit the gasifier in gaseous form. The composition of the products of the pyrolysis reactions r_{p1} and r_{p2}, taken from [1] and [15], are listed in Table I.

Table I: Product fractions (wt%) of the pyrolysis reactions [1, 15]

	CO	CO_2	H_2O	CH_4	H_2	tar	char
r_{p1}	4.5	10	11.5	0.3	0.2	48	25.5
r_{p2}	53.4	8.5	17	21.1	-	-	-

The data regarding r_{p1} listed in Table I have been derived from experiments performed with beech wood particles. Sufficient experimental data for pyrolysis of softwood pellets could not be obtained. Kinetic constants for the primary reactions are taken from [17] and for the cracking reaction (Eq. 16) of the tars constants are taken from [15]. Tar is modelled as a lumped hydrocarbon with the proposed composition C_6H_8O [16] and a molecular weight of 96. The reaction heat of the pyrolysis is assumed to be small and negligible (as supposed for r_{p2}) compared to the heat of reaction related to combustion and gasification [13]. For the primary pyrolysis a reaction heat of 300 kJ/kg (endothermic) has been assumed.

The homogeneous water-gas (Eq. 17) shift reaction is active in the pyrolysis and the drying zone as well and is modelled as a 1st order kinetic equation (Eq. 18) [26].

$$CO + H_2O \rightarrow CO_2 + H_2 \quad (17)$$

$$r_{wg} = X_{CO} * X_{H_2O} * A_{wg} * \exp\left(-\frac{E_{wg}}{R * T_{gas}}\right) \quad (18)$$

Kinetic constants of all reactions mentioned so far are listed in Table II.

2.3.3 Gasification

In the gasification or reduction zone the model includes the heterogeneous reactions of the char. The char is modelled as hydrocarbon $CH_{0.2526}O_{0.0237}$ [1] consisting primarily of carbon with small amounts of hydrogen and oxygen (elemental composition C =95 wt.%, H =2wt.%, O=3 wt.%). The following reactions are considered.

$$CH_{0.2526}O_{0.0237} + 0.9763H_2O \rightarrow CO + 1.1026H_2 \quad (19)$$

$$CH_{0.2526}O_{0.0237} + CO_2 \rightarrow 2CO + 0.1026H_2 + 0.0237H_2O \quad (20)$$

$$CH_{0.2526}O_{0.0237} + 1.8974H_2 \rightarrow CH_4 + 0.0237H_2O \quad (21)$$

The reaction rate of a heterogeneous reaction depends on several effects (e.g. mass transfer in the gas phase, diffusion or chemical reaction). To account for these effects an overall reaction rate (Eq. 22), depending on the mass transfer coefficient, the chemical reaction rate, the molar concentration of reacting gas phase species (H_2O, CO_2 and H_2) and the particle surface, is introduced.

$$r_{g,i} = \frac{X_i}{\frac{1}{k_d} + \frac{1}{r_{chem,g,i}}} * A_P \qquad with\ i = H_2O, CO_2, H_2 \quad (22)$$

Kinetic constants (listed in Table II) for the gasification reactions are taken from [18]. A literature correlation, taken from [21], is used for the mass transfer coefficient (Eq.23).

$$k_d = \frac{2.06 * v_{gas}}{\varepsilon} * \mathrm{Re}^{-0.575} * \mathrm{Pr}^{-\frac{2}{3}} \quad (23)$$

The values for the heat of reaction of the gasification reactions, listed in Table II, are derived from [20].

2.3.4 Combustion

In the combustion zone the biomass char is oxidized with the supplied air. Volatile products formed are burnt with oxygen to some extent. The combustion of char is a heterogeneous reaction. Similarly to the gasification reactions an overall reaction rate (Eq. 24) is introduced. However, it has been proven that char combustion is predominantly controlled by diffusion rather than kinetics [11, 23], so the chemical reaction rate (k_{c1}) of the reaction can be assumed to be irrelevant.

$$r_{c1} = \frac{p_{O_2}}{\frac{1}{(2 * k_{ox})} + \frac{1}{\left(\frac{M_{gas}}{M_{solid}} * r_{chem,c1}\right)}} * A_P \quad (24)$$

Kinetic constants for the combustion reaction (r_{c1}) are taken from [22]. A literature correlation, taken from [12], is used for the mass transfer coefficient (Eq.25).

$$k_{ox} = \frac{1.57 * v_{gas} * \rho_{gas} * Sc^{-\frac{2}{3}} * \mathrm{Re}^{-0.41} * (1-\varepsilon)^{0.2}}{M_{gas} * p} \quad (25)$$

The products of the char combustion are CO, CO_2 and water vapour (Eq.26), the stoichiometric coefficients can be calculated as

$$CH_{0.2526}O_{0.0237} + \left(1 - 0.5\chi + \frac{0.2526}{4} - \frac{0.0237}{2}\right)O_2 \rightarrow \chi CO + (1-\chi)CO_2 + \frac{0.2526}{2}H_2O \quad (26)$$

The CO/CO_2 –ratio χ depends on the actual combustion temperature (Boudouard equilibrium) and can be evaluated from Eq. 27 [3].

$$\chi = \left(\frac{k_{cc}}{1+k_{cc}}\right) \quad with \quad k_{cc} = 2500 * \exp\left(-\frac{6420}{T_{solid}}\right) \tag{27}$$

CO leaves the particle surface and is partly oxidized to CO_2 in the gas phase according to the following reaction (Eq. 28). The reaction rate of the CO combustion (Eq. 24) is derived from [11].

$$CO + 0.5CO_2 \rightarrow CO_2 \tag{28}$$

$$r_{c2} = \varepsilon * A_{c2} * X_{CO} * \left(X_{O_2}\right)^{0.5} * \left(X_{H_2O}\right)^{0.5} * \exp\left(-\frac{E_{c2}}{T_{gas}}\right) \tag{29}$$

Due to high combustion temperatures heterogeneous gasification reactions are already active in the combustion zone. Volatile products of these reactions leaving the particles are oxidized in the gas phase. The following homogeneous gas phase reactions are considered (Eq. 30 and Eq.31)

$$CH_4 + 2O_2 \rightarrow CO_2 + 2H_2O \tag{30}$$

$$H_2 + 0.5O_2 \rightarrow H_2O \tag{31}$$

The homogeneous gas phase reactions [27] are modelled as shown in equations 32 and 33.

$$r_{c3} = \varepsilon * A_{c3} * X_{CH_4} * X_{O_2} * \exp\left(-\frac{E_{c3}}{T_{gas}}\right) \tag{32}$$

$$r_{c4} = \varepsilon * A_{c4} * X_{H_2} * X_{O_2} * \exp\left(-\frac{E_{c4}}{T_{gas}}\right) \tag{33}$$

Kinetic data for the methane combustion and for the hydrogen combustion are derived from [27]. All relevant kinetic data and heats of reaction for the combustion reactions are listed in Table II.

Table II: Reference values for kinetic constants and heat of reaction

Reaction		A	Unit	E [J kmol^{-1}]	ΔH_R	Unit	Reference
m_{water}	(13)	$5.56x10^6$	s^{-1}	$8.79x10^7$	2250	kJ kg^{-1}	[10]
r_{p1}	(14)	$10^{4.03}$	s^{-1}	77800	350	kJ kg^{-1}	[17]
r_{p2}	(16)	$2.076x10^3$	s^{-1}	$66.3x10^6$	0	-	[15]
r_{wg}	(18)	1389	s^{-1}	$1.256x10^7$	-41.2	kJ mol^{-1}	[26]
r_{g1}	(19)	10^7	m s^{-1} K^{-1}	$1.256x10^8$	172.6	kJ mol^{-1}	[18, 20]
r_{g2}	(20)	10^7	m s^{-1} K^{-1}	$1.256x10^8$	131.4	kJ mol^{-1}	[18, 20]
r_{g3}	(21)	10^4	m s^{-1} K^{-1}	$1.256x10^8$	-75	kJ mol^{-1}	[18, 20]
r_{c1}	(24)	4750	kg m^2 s^{-1}	$2x10^8$	-110.6/393.8	kJ mol^{-1}	[22]
r_{c2}	(29)	$1.3x10^{11}$	kmol m^3 s^{-1}	$1.256x10^8$	-283	kJ mol^{-1}	[11]
r_{c3}	(32)	$2.552x10^{14}$	m^3 K^{-1} mol^{-1} s^{-1}	$9.304x10^7$	-808.5	kJ mol^{-1}	[27]
r_{c4}	(33)	$8.83x10^8$	m^3 K^{-1} mol^{-1} s^{-1}	$9.976x10^7$	-241.7	kJ mol^{-1}	[27]

2.3 Physical properties

Heat capacities of all species of the solid phase and for vapour tar are listed in Table III.

Table III: Reference values for heat capacities

	cp [kJ kg^{-1} K^{-1}]	Reference
biomass (dry)	1.38	[17]
char	$(420+2.09*T_{solid}+6.85*10^4*T^2_{solid})*10^3$	[17]
tar (vapour)	3.22	[12]
water	4.2	[12]

The heat capacities of the gas phase species except for tar have been fitted from data taken from literature [28] by means of 4th order polynomials and are not listed in Table III.

Thermal conductivity (Eq. 34) and viscosity (Eq. 35) of the gas are derived from [12].

$$\lambda_{gas} = \varepsilon * 4.8 * 10^{-4} * T_{gas}^{0.717} \tag{34}$$

$$\mu_{gas} = 1.98 * 10^{-5} * \left(\frac{T_{gas}}{300}\right)^{\frac{2}{3}} \tag{35}$$

The effective thermal conductivity of the solid phase consists of the thermal conductivities of the individual species. In addition, due to expected high temperatures in the gasification and oxidation zone, radiation can not be neglected and is taken into account by the thermal conductivity of the char. The effective thermal conductivity is modelled based on literature data derived from [10], [17] and [29].

$$\lambda_{solid} = k_{s0} * (\rho_{biomass,\ dry} + \rho_{water}) * 1/(\rho_{biomass,\ dry} + \rho_{water} + \rho_{char}) + k_{char} * \rho_{char} / (\rho_{biomass,\ dry} + \rho_{water} + \rho_{char}) \tag{36}$$

$$k_{s0} = 0.144 * \left(1.39 + 2.8 * 0.08 + 0.165) * \frac{\rho_{s0}}{1000}\right) \tag{37}$$

$$k_{char} = 0.5 * k_{red,gas} + \frac{\varepsilon * 0.1046}{\left[\frac{0.1046}{\left(d_p * k_{rad,solid}\right)}\right] + 1.43 * \left(1 - 1.2 * \varepsilon\right)} \tag{38}$$

$$k_{rad,gas} = 4 * \sigma * 0.05 * T_{gas}^3 \tag{39}$$

$$k_{rad,solid} = 4 * \sigma * 0.85 * T_{solid}^3 \tag{40}$$

2.4 Numerical solution

One basic objective of the model processing was to find a simple but sufficiently accurate numerical solution for the model equations. Focusing on steady state operation, the model is described by a set of highly non-linear, coupled, first order differential equations, that normally can be solved by an explicit finite difference method. Due to the countercurrent nature of the gas and solid flows resulting in a split-boundary value problem the model was solved by a developed code using a two step iterative method. In the first step guess values are used for the unknown boundary values on the top of the gasifier, as the simulation starts at the top of the gasifier (Fig. 1), and the model equations are solved by an ODE-

solver (ode23) based on an explicit Runge-Kutta (2,3) method [30]. In the second step the unknown boundary values are varied using the secant method [31], until all boundary conditions at the top and at the bottom of the gasifier are satisfied. However, other iterative methods like the Newton's method converge faster, but the Newton's method requires the evaluation of both, function and its derivative at every step, while the secant method only requires the evaluation of the function itself. Since the evaluation of the derivatives of all governing equations is quite time-consuming and error-prone, the secant method was chosen for the iterative step.

At the top of the packed bed (z=0) only solid phase properties are specified (Eq. 42), as the composition and the temperature of the producer gas are unknown.

$$T_{solid} = T_0 \tag{42.1}$$

$$\rho_{solid} = \rho_{solid,0} + \rho_{water} \tag{42.2}$$

$$\frac{\partial T_{gas}}{\partial z} = \frac{\partial T_{solid}}{\partial z} = 0 \tag{42.3}$$

At the bottom of the gasifier (z=L) the inlet air composition, temperature and mass flux of the gas phase are specified (Eq. 43). The solid ash is assumed to be at ambient temperature, the solid mass flux can be related to the initial ash content of the biomass.

$$T_{gas} = T_{solid} = T_0 \tag{43.1}$$

$$\rho_i = 0 \quad with \quad i = CO, CO_2, H_2, CH_4, tar \tag{43.2}$$

$$X_{O_2} = 0.21 \quad X_{N_2} = 0.785 \quad X_{H_2O} = 0.005 \tag{43.3}$$

3 RESULTS

The model is used to simulate a laboratory scale fixed-bed updraft gasifier.

3.1 Input parameter

Simulations have been carried out with the input parameters listed in Table IV for steady-state operation. The gasifier (Figure 2) consists of a cylindrical shaft, covered with an insulation made of ceramic fibres, and with an inner diameter of 0.125 m and a length of 0.6 m. The pellets are fed periodically to the gasifier in order to keep the bed at a constant height of approx. 0.45 m. Ash is periodically discharged from the grate to obtain continuous operation of the gasifier.

Table IV: Input parameters for the simulation of the gasifier

	value
T_0	293K
solid mass	3.5 kg h^{-1}
ρ_{s0}	650 kg m^{-3}
Y_{water}	8 wt%
Y_{ash}	0.5 wt% (db)
air to fuel ratio	1.45 kg kg^{-1} (wb)
ζ	0.5
ε	0.5
D	0.125 m
L	0.42 m

The results of the simulation are compared with measurements derived from test runs performed with the laboratory-scale fixed-bed updraft gasifier. The temperature inside the gasifier has been measured by a set of thermocouples (Type K). To avoid channelling, the thermocouples have been stuck into the packed bed only periodically to measure the temperature in the middle of the bed at intervals of 5 cm.

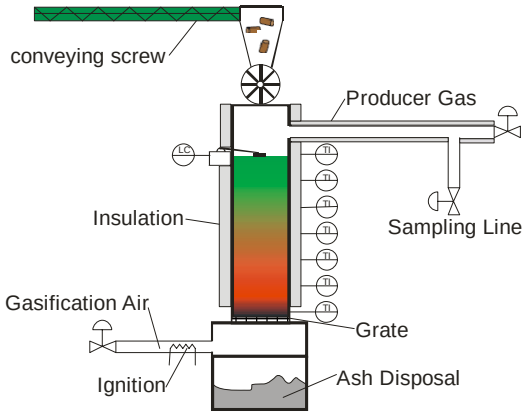

Figure 2: Investigated small-scale updraft fixed-bed gasifier

Samples of the producer gas have been repeatedly taken at the outlet of the gasifier by means of gas collection tubes. The samples have been cooled down to ambient temperature to remove tars. The composition of the producer gas was then measured by a micro Gas Chromatograph (CO, CO_2, H_2, CH_4, O_2 and N_2). The tar content of the producer gas was measured using a gravimetric method (solvent sampling train, vacuum drier).

3.2 Simulation results

In the Figures 3, 4 and 5 results of the simulations performed are shown. Figure 3 shows the axial temperature profiles of the solid and the gas phase compared with the measurements taken from test runs. The axial profiles of the gas phase species are illustrated in Figure 4. Figure 5 shows the axial profiles of the species of the solid phase. As fed to the gasifier the solid fuel is heated up by the product gas and evaporation of fuel moisture starts. The exit temperature of the producer gas is about 450K, showing good agreement with the measurements.

At 500K pyrolysis of the fuel starts indicated by distinctive gradients of temperature profiles and the decomposition of the fuel forming char and volatiles respectively. Concentrations of the gas phase species increase rapidly in the pyrolysis zone apart from CO, which is the major product of the oxidation and gasification zone. There is no satisfying agreement with the measurements regarding the producer gas composition as shown in Figure 4. The calculated high tar content of the producer gas could not be observed during test runs. Due to low temperatures in the pyrolysis zone cracking reactions of the tars are negligible [32]. The composition of the primary pyrolysis reaction has been taken from [1], whereas reported data has been derived from test runs carried out with beech wood particles. The derived experimental data may not be suitable for softwood pellets and the operating conditions respectively. This problem will be discussed in detail later.

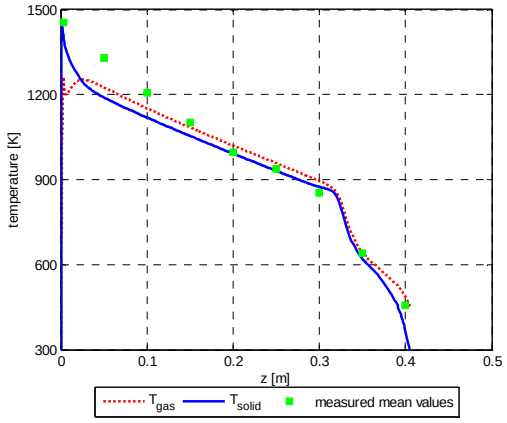

Figure 3: Axial profiles of solid and gas phase temperatures
Explanations: position of grate at z=0 m; gasification agent: air; bed height constant at 0.42 m

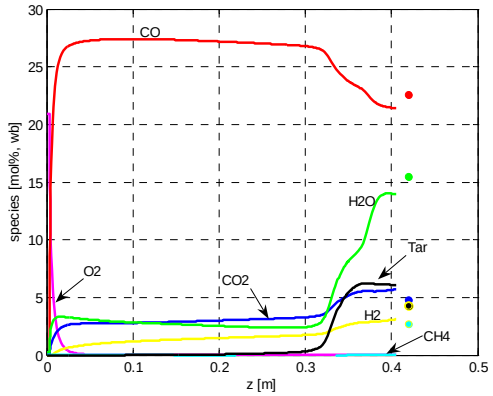

Figure 4: Axial profiles of gas phase species
Explanations: position of grate at z=0 m; gasification agent: air; bed height constant at 0.42 m

As drying and pyrolysis of the wood pellets is finished, the residual char particles are heated by the up-streaming hot gases. It seems that there is a long zone, situated in the middle of the gasifier, where homogeneous reactions are low and heterogeneous reactions do not occur (Figure 5). However, the water gas shift reaction is active, but the dominant process is the heating of the char bed by the hot gases coming from the bottom of the gasifier. This has been reported by other authors [1, 33] before and is in good agreement with measurements regarding the temperature profile.

Gasification and combustion are located along a thin zone at the bottom of the gasifier. As the air enters the gasifier, O_2 rapidly decreases as the char is burnt and the solid temperature attains high values. The steep gradients of the temperature profiles above the grate result from a very thin ash bed and because the air is supplied to the gasifier at ambient temperature. Consequently the difference between solid and gas temperature is high above the grate and the dominant process is the heterogeneous combustion of char resulting in high CO values as the gas phase reactions (combustion of CO) are slower due to the lower gas temperature. Due to the char combustion the solid temperature attains values slightly below 1500 K. As a result of the high temperature of the solid phase gasification of the char starts and the temperature of the solid phase decreases again due to the high endothermic nature of the gasification reactions. Again, CO is the major product of the gasification, the H_2 production is considerably small. The H_2 production could be increased by supplying humidified air or steam as gasification agent to the gasifier.

There no strict spatial breakup between combustion and gasification zone as competing reactions overlap each other. Heterogeneous gasification reactions start due to high temperature of the solid char although char combustion is still active. About 5 cm above the grate combustion reactions terminate indicated by the complete extinction of oxygen. Consequently the solid und gas temperatures decrease due to the endothermic gasification reactions and all heterogeneous reactions expire.

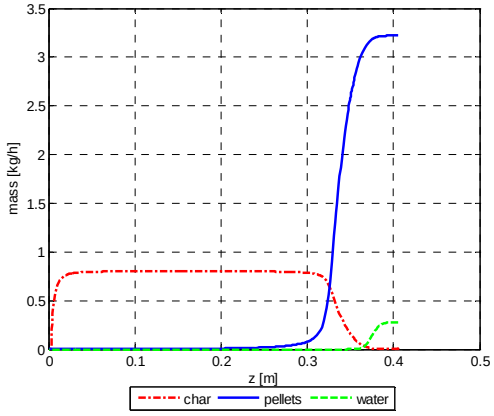

Figure 5: Axial profiles of solid phase species
Explanations: position of grate at z=0 m; gasification agent: air; bed height constant at 0.42 m

3.3 Evaluation of pyrolysis

As already discussed no good agreement is achieved between prediction and measurement for the composition of the producer gas of the gasifier, probably caused by inadequate experimental data for the pyrolysis zone. The product composition of the primary pyrolysis reaction strongly depends on the boundary conditions (e.g. heating rate, reactor temperature) of the experiment and of course the fuel itself. The predicted tar content of the producer gas was considerably higher than the repeatedly measured value derived from test runs.

Therefore, the product composition of the primary pyrolysis reaction has been adapted as follows. As it is well-known, tars often undergo secondary cracking reactions forming lighter gases. Due to the moderate temperatures in the upper region of the packed bed of the gasifier, cracking of tars, as described by the model with the temperature depending reaction r_{p2}, does not occur. Therefore, the predicted tar content of the producer gas depends just on the product composition of the primary pyrolysis reaction. Since the boundary conditions of the experiment, the pyrolysis data have been derived from, differ from the conditions of the test runs performed with the laboratory-scale gasifier, the producer gas composition can only be influenced by changing the product composition of the primary pyrolysis reaction. Therefore, the tar ratio of the primary pyrolysis reaction has been reduced to fit to measured values and the remaining reported tar ratio undergoes a secondary reaction as described by [15]. Furthermore, the secondary cracking reaction (r_{p2}) is not taken into account

for the simulation. The modified composition of the pyrolysis products is listed in Table V.

Table V: Reported and modified mass fractions (wt%) of the primary pyrolysis reaction [1, 15]

	CO	CO_2	H_2O	CH_4	H_2	tar	char
r_{p1}	4.5	10	11.5	0.3	0.2	48	25.5
r_{p1}	11.7	11.1	13.8	3.2	0.2	34.5	25.5

Based on the new input data for the pyrolysis zone, simulations of the gasifier have been performed again. Remaining input parameters, listed in Table III, have not been changed. Figure 6 shows the axial profiles of the gas phase species based on the new parameters for pyrolysis. Due to the changed pyrolysis data the predicted composition of the product gas is now in good agreement with the measurements despite of an acceptable deviation related to CO_2 and H_2. The influence of the modified data on the temperature profiles of the solid and the gas phases is small as shown in Figure 7. The outlet temperature of the producer gas decreases about 5K due to the changed gas phase enthalpies in the pyrolysis zone.

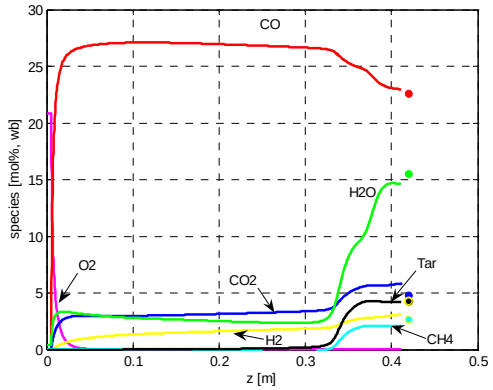

Figure 6: Axial profiles of gas phase species
Explanations: position of grate at z=0 m; gasification agent: air; bed height constant at 0.42 m

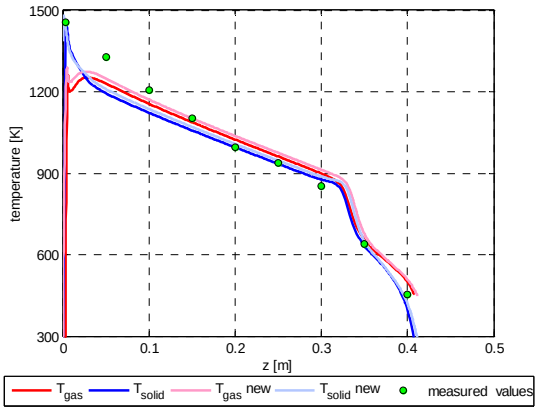

Figure 7: Axial profiles of solid and gas phase temperatures
Explanations: position of grate at z=0 m; gasification agent: air; bed height constant at 0.42 m

4 CONCLUSIONS

A one-dimensional steady state mathematical model for small scale fixed-bed updraft gasifiers operated with softwood pellets has been developed and solved. The model is based on a set of differential equations solved by a two step iterative method. Chemical and physical properties of the gasification process have been derived from literature and implemented into the model. Simulations have been carried out for a laboratory-scale fixed-bed updraft gasifier and simulation results have been compared to measurements derived from test runs performed.

Basically, good agreement is obtained between calculated and experimental results regarding the axial temperature profiles. However, the prediction of the composition of the producer gas is imprecise, probably caused by the simplified description of pyrolysis and insufficient data for the pyrolysis of softwood pellets. Primarily, the predicted high tar content could not be observed during test runs.

Therefore, the tar ratio of the primary pyrolysis reaction has been reduced to fit to measured values and the remaining reported tar ratio undergoes a secondary reaction forming lighter gases as described by [15]. Due to the changed pyrolysis data the predicted composition of the product gas is in good agreement with the measurements despite of a deviation related to CO_2 and H_2. The treatment of the pyrolyis zone may be the weakest part of the model, but more experimental data are required in order to achieve improvements.

The simulation model enables a good quantitative prediction of the small-scale updraft fixed-bed gasifier. The gasifier model can be a useful tool for the prediction of the temperature profiles and relevant output variables like producer gas composition and the air to fuel ratio as well as particularly for a proper reactor design. Continued experimental and modelling work is ongoing in order to further improve the model.

5 NOTATIONS

A_i	preexponential factor
A_p	particle surface area (m^2)
cp	heat capacity (kJ kg^{-1} K^{-1})
D_V	reactor diameter (m)
d_p	particle diameter (m)
E_i	activation energy (J $kmol^{-1}$)
k_i	mass transfer coefficient
L	length of fuel bed (m)
M_i	molecular weight (kg $kmol^{-1}$)
m_{water}	mass flow water (kg h^{-1})
p	pressure (Pa)
Pr	Prandtl number
R	universal gas constant (J $kmol^{-1}$ K^{-1})
r_i	reaction rate (kmol m^{-3} s^{-1}, kg m^{-3} s^{-1})
Re	Reynolds number
Sc	Schmidt number
s_h	heat transport
s_q	heat transfer
T	temperature (K)
u	storage term
v	velocity (m s^{-1})
W	heat flux (kJ s^{-1})
X	molar concentration (kmol $kmol^{-1}$)
Y	mass concentration (kg kg^{-1})

Greek letters

α_w	heat transfer coefficient (kJ m^{-2} s^{-1} K^{-1})
ΔH	reaction heat (kJ kg^{-1}, kJ $kmol^{-1}$)
ε	bed porosity
ζ	correction factor for heat transfer
λ	thermal conductivity (W m^{-1} K_{-}^{1})
μ	gas viscosity (N s m^{-2})
ρ	mass concentration (kg m^{-3}) for gas and apparent density for solid (kg m^{-3})
σ	Stefan-Boltzmann-constant (W m^{-2} K^{-4})
χ	CO-CO_2 ratio

Subscripts

c	combustion reactions
CO	carbon monoxide
chem	chemical reaction
dry	dry base
g	gasification reactions
gas	gas phase
gw	gas to wall
H_2O	water vapour
i	species
ox	combustion reaction 1
p1	primary pyrolysis
p2	secondary pyrolysis
sg	solid to gas
solid	solid phase
sw	solid to wall
w	reactor wall
wg	water gas shift
0	ambient or initial value

6 REFERENCES

[1] C. Di Blasi, Modeling Wood Gasification in a Countercurrent Fixed-Bed Reactor, A.I.Ch.E. Journal, Vol. 50, No. 9 (2004)

[2] T. K. Kayal," M. Chakravarty & G. K. Biswas; Mathematical modelling of steady state updraft gasification of jute stick particles of definite sizes packed randomly – an analytical approach, Bioresource Technology 60 (1997), 131-141

[3] C. Lucas, High temperature air/steam gasification of biomass in an updraft fixed bed batch type gasifier; Ph. D. Thesis (2005), KTH

[4] M. Usman Ghani, Predrag T. Radulovic and L. Douglas Smoot; An improved model for fixed-bed coal combustion and gasification: sensitivity analysis and applications, Fuel Vol. 75, No. 10 (1996), pp 1213-1226

[5] M. Brundo, A mathematical model for coal and biomass gasification in a fixed bed reactor, 3rd International Conference on Clean Coal Technologies for our Future (2007)

[6] Hobbs, M. L., Radulovic, P. T., &Smoot, L. D., Combustion and gasification of coals in fixed beds. Progress Energy and Combustion Science, 19 (1993), 505-586.

[7] Hobbs, M. L., Radulovic, P. T., & Smoot, L. D., Modelling fixed-bed coal gasifiers. A.I.Ch.E. Journal, 38 (1992), pp 681-702.

[8] L.A. Gould, Chemical Process Control: Theory and Applications. Addison Wesley (1969)

[9] M. Bellais, Modelling of the pyrolysis of large wood particles, Ph. D. Thesis (2007), KTH, Stockholm

[10] D. J. Purnomo, Model for a Downdraft Solid Fuel Combustor, Ph. D. Thesis (1998), The University of Wisconsin

[11] J.Cooper, W.L.H. Hallett, A numerical model for packed-bed combustion of char particles, Chemical Engineering Science 55 (2000), pp 4451-4460

[12] Rosa, L., Tosato, R.; Modelling and testing a cogeneration plant based on wood gasification; 7th European Conference on Industrial Furnaces and Boilers, 2006

[13] Rath, J. et al.; Heat of wood pyrolysis, Fuel 82, 81–91, 2003

[14] Di Blasi, C., Signorelli, G., Portoricco, G.; Countercurrent Fixed-Bed Gasification of Biomass at Laboratory Scale; Ind. Eng. Chem. Res. 1999, 38, 2571-2581

[15] Rath, J., Staudinger, G.; Cracking reactions of tar from pyrolyis of spruce wood, Fuel 80 2001, pp 1379-1389

[16] H. Thunman, F. Niklasson, F. Johnsson,B. Leckner, Composition of Volatile Gases and Thermochemical Properties of Wood for Modeling of Fixed or Fluidized Beds, Energy Fuels, Vol. 15 (2001), pp 1488 -1497

[17] M. Grønli, A theoretical and experimental study of the thermal degradation of biomass, Ph. D. Thesis (1996), NTNU, Trondheim

[18] M. J. Groeneveld, W.P.M. van SwaaiJ, Gasification of char particles with CO_2 and H_2O, Chem.Eng.Science Vol. 35 (1980), pp 307-313

[19] Y. Wang, C.M. Kinoshita, Kinetic model of biomass gasification

[20] B.V. Babu , Pratik N. Sheth, Modeling and simulation of reduction zone of downdraft biomass gasifier: Effect of char reactivity factor, Energy Conversion&Management (2005)

[21] M. Usman Ghani et al., Fbed-1: Fixed Bed Coal Combustion and Gasification Model with a Generalized Coal Devolatilization Submodel (FG-DVC), Measurement and Modeling of Advanced Coal Conversion Processes, Vol. III (1993)

[22] P. M. Bhagat, Wood charcoal combustion and the effects of water application, Combustion and Flame, Vol. 37 (1980), pp 275-291

[23] R. Bauer et al., Modelling of grate combustion in a medium scale biomass furnace for control purpose, submitted!

[24] K. M. Bryden, K. W. Ragland, Numerical Modeling of a Deep, Fixed Bed Combustor, Energy & Fuels, Vol. 10 (1996), pp 269-275

[25] H. Raupenstrauch, Ein Beitrag zur Computersimulation reagierender Schüttschichten, Ph. D. Thesis (1991), Technische Universität Graz

[26] V. Biba, J. Macak, E. Klose, J. Malecha, Mathematical model for the gasification of coal under pressure. Ind. Eng. Chem. Process Des. Dev., Vol. 17 (1978), pp 92–8.

[27] Z. Deng et al., Computational Fluid Dynamics Modeling of Coal Gasification in a Pressurized Spout-Fluid Bed, Energy & Fuels, Vol. 22 (2008), pp 1560–1569

[28] VDI-Wärmeatlas, Verein deutscher Ingenieure, Springer Verlag (1997)

[29] J. Goldman et al. , A comparison of prediction and experiment in the gasification of anthracite in air and oxygen-enriched/steam mixtures, 20th Symposium (International) on Combustion, pp 1365-1372
[30] P. Bogacki, L. F. Shampine, A 3(2) pair of Runge-Kutta formulas, Appl. Math. Letters, Vol. 2 (1989), pp 1-9
[31] H.-J. Bartsch, Taschenbuch mathematischer Formeln, 19. Auflage (2001), Fachbuchverlag Leipzig im Carl Hanser Verlag
[32] P.O. Morf, Secondary Reactions of Tar during Thermochemical Biomass Conversion, Ph. D. Thesis (2001), ETH Zürich
[33] H. Raupenstrauch, Gasdurchströmte chemisch reagierende Schüttschichten, Habilitationsschrift (1997), Technische Universität Graz

7 ACKNOWLEDGEMENTS

- The financial support of the Austrian Research Promotion Agency (FFG) is gratefully acknowledged.

8 LOGO SPACE